Temperature dependence of magnetization reversal mechanism in misch-metal substituted Nd-Fe-B magnets sintered by dual alloy method

Dan Liu [a,*], JieFu Xiong [b], Lichen Wang [b], Xinqi Zheng [c], Fei Peng [a], Xi Ming [b], Tongyun Zhao [d], Fengxia Hu [d], Jirong Sun [d], Baogen Shen [b,d,*], Jun Shen [e,*]

[a] Department of Physics, Beijing Technology and Business University, Beijing 100048, PR China
[b] Ningbo Institute of Materials Technology & Engineering, Chinese Academy of Sciences, Zhejiang 315201, PR China
[c] School of Materials Science and Engineering, University of Science and Technology Beijing, Beijing 100083, PR China
[d] State Key Laboratory of Magnetism, Institute of Physics, Chinese Academy of Sciences, Beijing 100190, PR China
[e] School of Mechanical Engineering, Beijing Institute of Technology, Beijing 100081, PR China

ARTICLE INFO

ABSTRACT

The substitution of Nd by misch-metal (MM) in Nd-Fe-B permanent magnets has attracted extensive attention due to the effective reduction of production cost and rational utilization of rare earth resources. In particular, multi-main phase (MMP) magnets prepared by dual alloy method possess a higher permanent magnetic performance than that of single main phase (SMP) magnets. However, the coercivity mechanism of MMP magnets is different from the nucleation and propagation of SMP magnets, especially the interactions of different 2:14:1 main phases have not been clarified. In this study, we investigated the temperature dependence of magnetization reversal mechanism in (MM,Nd)-Fe-B magnets by using recoil loops, minor hysteresis loops, first-order and second-order reversal curves. It found that with the increase of temperature, the magnetic moments motion is mainly affected by long-range magnetostatic interaction rather than exchange coupling. The weakened coupling interaction makes the demagnetization process of softer and harder magnetic phases asynchronous. The thermal activation energy barrier index related to coercivity mechanism is 1.45, 1.18 and 1.0 at 200 K, 300 K and 380 K, respectively. It indicates that nucleation and expansion of reversed domains are the main mechanisms controlling the magnetization reversal process at low temperature. While the coercivity at high temperature is mainly determined by the domain wall pinning mechanism. In addition, we noted that both two coercivity mechanisms coexist in MMP magnets at 300 K. Micromagnetism has also been used to verify the coercivity mechanism of (MM,Nd)-Fe-B magnets sintered by dual alloy method, which is of great significance for improving the magnetic properties of high abundance rare earth magnets.

1. Introduction

Nd$_2$Fe$_{14}$B-based magnets have been the most widely used permanent magnets since they were discovered due to their excellent permanent magnetic performance at room temperature [1–3]. In order to rationally utilize rare earth resources and effectively reduce production cost, the replacement of Nd by misch-metal (MM) has become the focus of attention [4,5]. However, the magnetic properties of (MM,Nd)-Fe-B magnets deteriorate drastically due to the inferior intrinsic properties of MM$_2$Fe$_{14}$B. Compared with the traditional single alloy method, the dual alloy method by mixing MM$_2$Fe$_{14}$B with Nd$_2$Fe$_{14}$B powders has an obvious advantage in preparing high performance rare earth permanent magnets [6–8]. The mixed sintering of two powders can form the microstructure of multi-main phase (MMP) magnet, which greatly improves its coercivity and magnetic properties. The different interactions between internal grains and grain boundaries will make the permanent magnets have a more special coercivity mechanism. It is essential to understand the magnetization reversal process, which has a significant impact on the development of new permanent materials and provides guidance for improving the performance of magnets.

According to the different characteristics of magnetization reversal process, the coercivity mechanism can be divided into uniform rotation, nucleation, domain wall pinning and thermal activation. For traditional sintered Nd-Fe-B magnets with single phase, the coercivity mechanism is

---

* Corresponding authors.
  E-mail address: liudan@btbu.edu.cn (D. Liu).

generally considered to belong to the nucleation type [9]. Anisotropy, surface defects, grain boundary conditions and magnetism are the key factors that affect the properties of magnets. However, most relevant reports are based on phenomenological empirical formulas, which are difficult to penetrate to the microscopic level. The inconsistency of macroscopic manifestation and microscopic interpretation makes the coercivity mechanism of traditional SMP magnet not universal [10–12]. Meanwhile, the reports on MMP sintered magnets mostly focus on the permanent magnet properties such as magnetic energy product and coercivity, and rarely involve the magnetization and demagnetization process [11,13]. Xiong et al. preliminarily studied the magnetization reversal of (MM,Nd)-Fe-B magnets with different MM contents through the phase structure, microstructure structure and magnetic properties [14]. It is considered that domain nucleation and growth are the main factors controlling the magnetization reversal process of (MM,Nd)-Fe-B MMP magnets. However, since (MM,Nd)-Fe-B is temperature sensitive, it is difficult to determine the coercivity mechanism of MMP magnets only from demagnetization process at room temperature. It is urgent to explore the changes of interactions within magnets at different temperatures and their effects on the coercivity mechanism, to understand the magnetization reversal process of high-abundance rare earth permanent materials, especially MMP sintered magnets.

In this work, the effect of temperature on magnetic properties and magnetization reversal process of (MM,Nd)-Fe-B magnets have been studied. The magnetization behavior and interaction between grains were analyzed from the initial magnetization curves, the recoil loops and the minor hysteresis loops. In addition, first-order and second-order reversal curves are powerful techniques for qualitative and quantitative identification of magnetic phases, which are very sensitive to the distribution of irreversible magnetization and reversed field [15–18]. The magnetism and interaction mechanism between different main phases were evaluated from multiple perspectives to fully understand the magnetization reversal process of high abundance rare earth magnets.

2. Experimental and simulation methods

The raw materials of $MM_{14}Fe_{79.9}B_{6.1}$ and $Nd_{13.5}Fe_{80.5}B_6$ were prepared by induction melting, strip casting, hydrogen decrepitating and jet milling. These two powders were mixed evenly at a mass ratio of 30:70 using the 3D mixer. The mixed powders were pressed and aligned under a pressure of 5 MPa and a magnetic field of 1.8 T, followed by isostatic compacting under a pressure of 160 MPa. Then the green compacts were sintered and annealed. An alloy with the atomic composition of $La_{1.18}Ce_{2.18}Pr_{0.21}Nd_{10.08}Fe_{80.32}B_{6.03}$, hereinafter defined as MM30, was prepared by a dual alloy method [14].

In order to study the coercive mechanism of magnets, several magnetization curves have been measured in this paper. Recoil loops refer to the changing process of magnetization with the external magnetic field increasing from zero to a certain value and then gradually decreasing to zero. Minor hysteresis loop is a series of hysteresis loops under different maximum magnetic fields, whose maximum external magnetic field is smaller than the saturation field of the sample. A single FORC is measured by the magnetization curve from a reversed magnetic field (H_R) to saturation in the positive direction [16]. The family of FORCs can be collected to fill the major loop by changing the H_R. The measurements and analysis methods of second-order reversal curve (SORC) are similar to FORC. The SORC measurement begins with a saturated magnetization state under a large positive external field. The field is reduced to a reversed field H_{R1}, and then increased to another field H_{R2}. The hysteresis curve between H_{R1} and H_{R2} is one of the SORCs. A series of SORCs with reversed fields H_{R1} can be obtained by changing the value of H_{R2} [19]. The sample used in the FORC measurement was formed into a cuboid of $0.8 \times 0.8 \times 3$ mm^3, with a geometrical long axis parallel to the z-axis. Different hysteresis loops were measured at 200 K, 300 K, and 380 K using a superconducting quantum interference device vibrating sample magnetometer (SQUID VSM, Quantum Design

MPMS-3). The magnets were demagnetized by high-frequency oscillating attenuated magnetic fields before the experiments. And the grains inside the magnet can maintain a single domain state during demagnetization and remagnetization after they are completely magnetized to saturation [9,20,21].

The theory of micromagnetism is an effective method to investigate the exchange coupling mechanism and coercivity mechanism of permanent magnets [22,23]. As shown in Eq. 1, the total Gibbs free energy (E_{tot}) of the system can be expressed by exchange energy E_{ex}, anisotropy energy E_{ani}, demagnetization energy E_d, and external field energy E_{ext} [24]:

$$E_{tot} = E_{ex} + E_{ani} + E_d + E_{ext}, \tag{1}$$

$$E_{tot} = \int \left\{ A\left[(\nabla \boldsymbol{m_x})^2 + (\nabla \boldsymbol{m_y})^2 + (\nabla \boldsymbol{m_z})^2 \right] - K_1 \boldsymbol{m_z^2} - \frac{1}{2}\mu_0 \boldsymbol{M} \cdot \boldsymbol{H_d} - \mu_0 \boldsymbol{M} \cdot \boldsymbol{H_{ext}} \right\} dV. \tag{2}$$

Where A, K_1 and V are the exchange integral constant, magnetocrystalline anisotropy constant and total volume of magnetic material, respectively. Magnetization $\boldsymbol{M}$ is used to describe the state of magnetization, which is a continuous function of position. $\boldsymbol{m_x} = \boldsymbol{M_x}/M_s$, $\boldsymbol{m_y} = \boldsymbol{M_y}/M_s$, and $\boldsymbol{m_z} = \boldsymbol{M_z}/M_s$ are the components of normalized magnetization. The demagnetization process and equilibrium domain structure of permanent magnet can be obtained by solving the minimum Gibbs energy of the system.

The model containing 100 irregular grains was constructed by Neper and the simulation was performed by finite element micromagnetics package Magpar [25,26]. The model is a cube with an edge length of 3000 nm, and 166460 cells are obtained by tetrahedral adaptive meshing method based on Delaunay algorithm [27]. In order to simplify the model, $Nd_2Fe_{14}B$ and $(Nd_{0.2}Ce_{0.8})_2Fe_{14}B$ were selected to represent Nd-Fe-B and MM-Fe-B, respectively. Material parameters used for the calculation are as follow [28,29]: for Nd-Fe-B, the anisotropy constant $K_1 = 4.30$ MJ/m^3, the saturation magnetization $J_s = 1.61$ T, and the exchange integral $A = 7.70$ pJ/m; for MM-Fe-B, $K_1 = 2.06$ MJ/m^3, $J_s = 1.25$ T, and $A = 2.48$ pJ/m. Consistent with the experiment, the ratio of these two grains in MM30 is 70:30.

3. Results and discussion

As shown in Fig. 1, the recoil loops of MM30 at different temperatures were obtained from the demagnetization state. During the initial magnetization process, the magnetization increases rapidly with the external field and changes slowly around the coercive field. As the external field continues to increase, the magnetization continues to increase until magnetization saturation, which is consistent with the nucleation mechanism. With the increase of temperature, the field required to achieve magnetization saturation increases and the step of initial magnetization curve gradually disappears. By comparing the arrows in Fig. 1(a) to (c), it can be seen that the recovery curve changes from flat to incline and the demagnetization curves become less steep at high temperature, which is a typical two-phase composite permanent magnet [7]. The magnetization reversal process of different phases is not consistent due to the weakening of coupling effect. The δm curves in Fig. 1(d) is defined as δm = $[M_d(H)+2M_r(H)]/M_r(\infty)$-1, which can be used to qualitatively characterize the interaction between uniaxial anisotropic particles with single domain [24]. Where $M_r(H)$ is isothermal remanent magnetization, obtained after the application and subsequent removal of a direct field H. And $M_d(H)$ is direct current demagnetization remanence, obtained after direct current saturation in one direction and the subsequent application and removal of a direct field H in the reverse direction. The intergrain interactions mainly include the long-range magnetostatic interaction and the exchange coupling interaction of neighboring grains. A positive value of δm means the exchange coupling plays a dominant role in magnetization reversal,
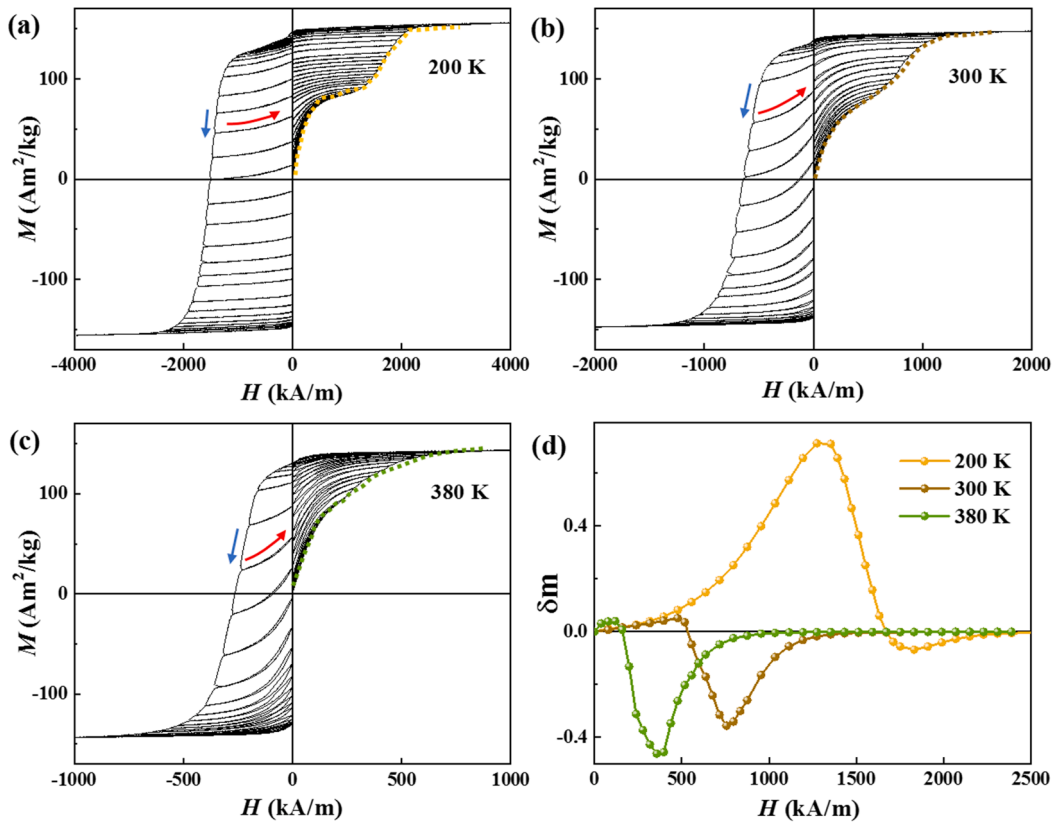
Fig. 1. Recoil loops of MM30 under different external magnetic fields were obtained at (a) 200 K, (b) 300 K, (c) 380 K. Blue and red arrows are used to characterize the trend of demagnetization curve and recovery curve, respectively. (d) δm curve is used to represent the interaction form within the material. The initial state of the magnet is an alternating current demagnetization state. (For interpretation of the references to colour in this figure legend, the reader is referred to the web version of this article.)

otherwise it is the long-range magnetostatic interaction. At 200 K, δm has a large positive value and only a small negative value even after $H > H_c$. However, the positive peak becomes very weak at high temperature, much smaller than the negative one. It shows that the coercivity mechanism of MM30 is changed and the motions of magnetic moments are mainly affected by long-range magnetostatic interaction rather than exchange coupling.

Since the first-order reversal curve (FORC) can completely record all irreversible magnetization processes, it is more conducive to understanding the intergrain interactions of MMP magnets. The normalized FORC distribution in Fig. 2 is defined as the mixed second order derivative of $M(H_R, H)$ with respect to H and H_R [30–32]:

$$\rho(H_R, H) = -\frac{1}{2M_s} \frac{\partial^2 M(H_R, H)}{\partial H_R \partial H}. \tag{3}$$

Any nonzero ρ in this two-dimensional contour map corresponds to an irreversible magnetization process. As we can see, the FORC distributions at different temperatures have similar overall shapes except for their relative positions and sizes. One peak located at the lower H corresponds to the irreversible magnetization of softer magnetic grains (MM$_2$Fe$_{14}$B), while the other peak corresponds to the harder magnetic grains (Nd$_2$Fe$_{14}$B). At 200 K, the peak of the former is very weak and almost negligible, which indicates that the magnetization reversal processes of two main phases are consistent and difficult to be distinguished by FORC distribution. The blue and red circles at high temperature represent the independent demagnetization process of different main phases. As shown in Table 1, the relative integral intensity of the softer main phase gradually increased from 8.95% at 200 K to 30.93% at 380 K. In other words, the irreversible magnetization component ratio of softer and harder phases is close to 3:7 at 380 K, which is in good

agreement with the mass ratio (30:70) of MM$_2$Fe$_{14}$B and Nd$_2$Fe$_{14}$B in MM30 magnet.

The region above the H_c-axis corresponds to the irreversible process in which the reverse field during remagnetization is greater than that during demagnetization. According to Table 1, the higher the temperature, the lower the relative integral intensity beyond H_c-axis, indicating that the coupling within the magnet becomes weaker. Fig. 2 (a) shows a very narrow distribution along the left diagonal (H_u-axis). When the temperature increases, the distribution along the H_u-axis becomes obvious, that is, the orientation or exchange coupling of the magnet has changed. Since the orientation of the same magnet is less affected by temperature, it is mainly caused by the change of exchange coupling between grains. The orientation of the grains along the easy axis is always about 14° at different temperature. However, when the exchange coupling is weak, the angular distribution will be clearly reflected near the diagonal. Therefore, the contour line near the H_u-axis also proves the exchange coupling inside the magnet gradually weakens with the increase in temperature.

Compared with the FORC diagram, the one-dimensional irreversibility distribution can be used to represent the magnetization reversal process more intuitively. The integral of ρ with respect to external magnetic field is also known as FORC switching field distribution (SFD) [15,24]:

$$\int \frac{\partial^2 M(H_R, H)}{\partial H_R \partial H} dH = \frac{\partial M(H_R)}{\partial H_R}. \tag{4}$$

The SFD in Fig. 3 shows the contribution of exchange coupling between the two main phases to the magnetization reversal. Red and blue dots are the reversed field distribution of harder and softer magnetic grains, respectively. The upper horizontal axis H_R/H_c represents the
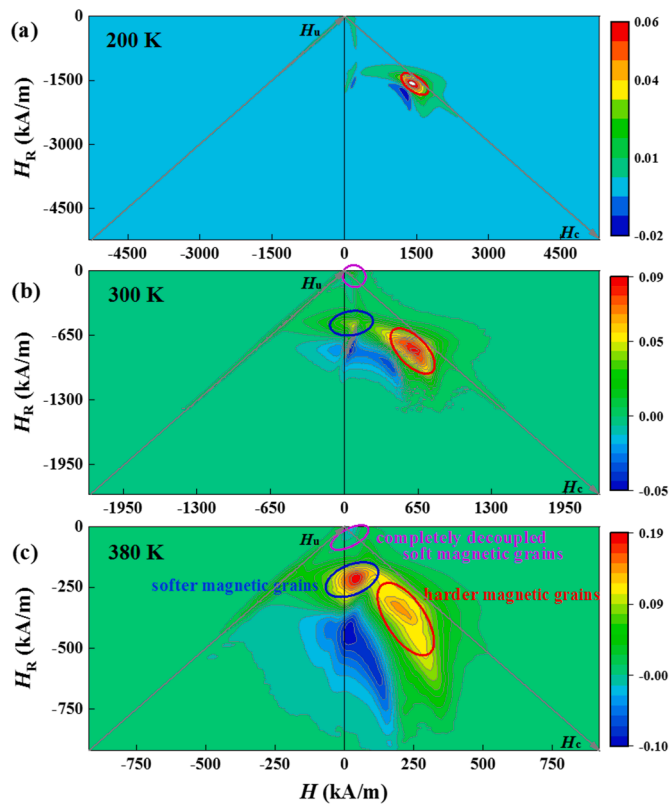
Fig. 2. Two-dimensional FORC distribution of MM30 at (a) 200 K, (b) 300 K and (c) 380 K. The corresponding FORC distributions are shown as contour plots after demagnetization correction. The blue and red solid lines represent peaks corresponding to magnetization reversals of most softer and harder magnetic grains. (For interpretation of the references to colour in this figure legend, the reader is referred to the web version of this article.)

Table 1
Relative intensities of integrals in different regions of the FORC distribution map.

Temperature (K)	Intensity of softer main phase	Intensity beyond the H_c-axis
200	8.95%	28.32%
300	21.58%	20.01%
380	30.93%	13.89%

reversed field normalized with respect to the corresponding coercive field. As shown in Fig. 3(a), the SFD of harder main phase almost coincides with that of the total magnet, indicating that $MM_2Fe_{14}B$ grains and $Nd_2Fe_{14}B$ grains can be well coupled at 200 K. The SFD of the magnet exhibits axisymmetric along the coercivity, which is single-phase behavior [14]. However, with the increase of temperature, SFDs of two kinds of grains gradually deviate from the symmetric distribution and become very dispersed. It means that the interaction within the magnet has changed and the magnetic domain of softer main phases cannot rotate consistently with harder main phase which supports the results of FORC distribution. In addition, the SFD corresponding to softer main phase has a negative value at $|H_R/H_c| > 1$, which also confirms the exchange coupling has weakened.

The interaction within the material changes significantly with temperature, which has a great impact on the magnetization reversal mechanism. The minor hysteresis loops in Fig. 4(a)~(c) can be used to reflect the gradual magnetization process of MM30 magnet at different temperatures. With the increase of temperature, the step near zero field becomes less obvious, and the coercivity and squareness of magnet become worse. The squareness is the ratio of H_k to H_c, where H_k is the
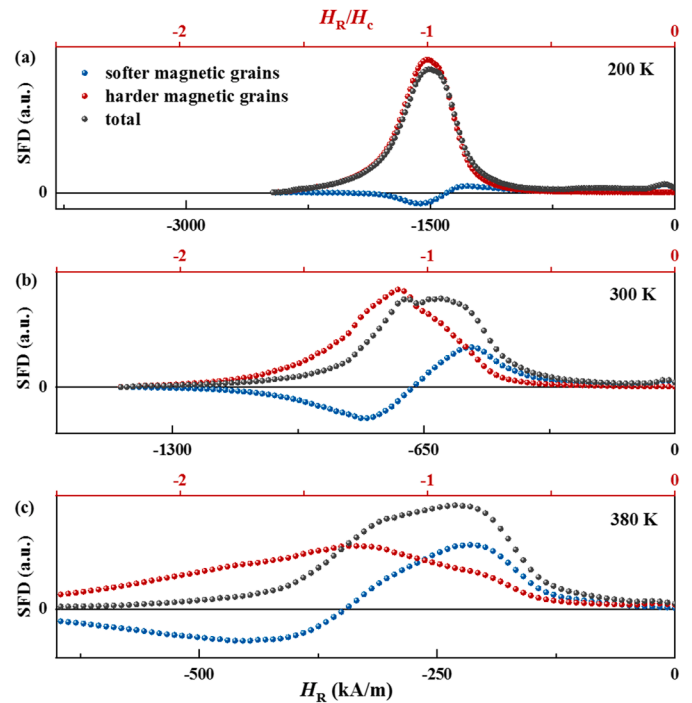
Fig. 3. FORC switching field distribution (SFD) of MM30 at (a) 200 K, (b) 300 K, and (c) 380K. The red, blue and black dotted lines are the reversed field distribution curves of the harder magnetic grains, softer magnetic grains and total magnet, respectively. The reversed field H_R and the normalized reversed field H_R/H_c are taken as the lower and upper abscissa respectively. (For interpretation of the references to colour in this figure legend, the reader is referred to the web version of this article.)

magnetic field corresponding to 0.9Br in the demagnetization curve. The squareness ranges from 0 to 1. The closer it is to 1, the better the anti-demagnetization ability of the magnet. The minor hysteresis loop is composed of a group of hysteresis loops with the magnetic field less than the saturation field. Fig. 4(d) shows the coercivity H_c^{minor} of each minor hysteresis loop as a function of magnetic field H, where the horizontal and vertical coordinates are normalized with respect to H_c. When $H/H_c = 1$, the H_c^{minor} at 200 K has reached 80% of the maximum coercivity, and rapidly reaches the maximum value with the external field increases. In this case, the nucleation and expansion of reversed domains are the main mechanisms controlling the demagnetization process. However, the H_c^{minor} at high temperature is less than 20% of the maximum coercivity when $H/H_c = 1$, and increases more slowly. The variation trend of the normalized remanence M_r^{minor}/M_r is similar to that of H_c^{minor}/H_c, indicating that the coercivity mechanism changes from the nucleation type to the pinning type with the temperature increases.

In essence, magnetization reversal is the process by which the magnet overcomes the energy barrier (E_b) from a metastable state to a steady state. When E_b is close to the thermal disturbance energy (k_BT) under the effect of external magnetic field, the magnetization reversal can be directly induced by crossing the E_b. The relationship between the energy barrier and the external magnetic field is [33]:

$$E_b(H) = E_0(1 - H/H_0)^n. \qquad (5)$$

Taking the derivative of Eq. (5) with respect to external magnetic field H, the change rate of the energy barrier at the coercivity with the H can be obtained:

$$\left. \frac{\partial E_b}{\partial H} \right|_{H=H_c} = -n\frac{E_0}{H_0}\left(1 - \frac{H_c}{H_0}\right)^{n-1}. \qquad (6)$$

Where E_0 is the energy barrier without external magnetic field, and H_0 is
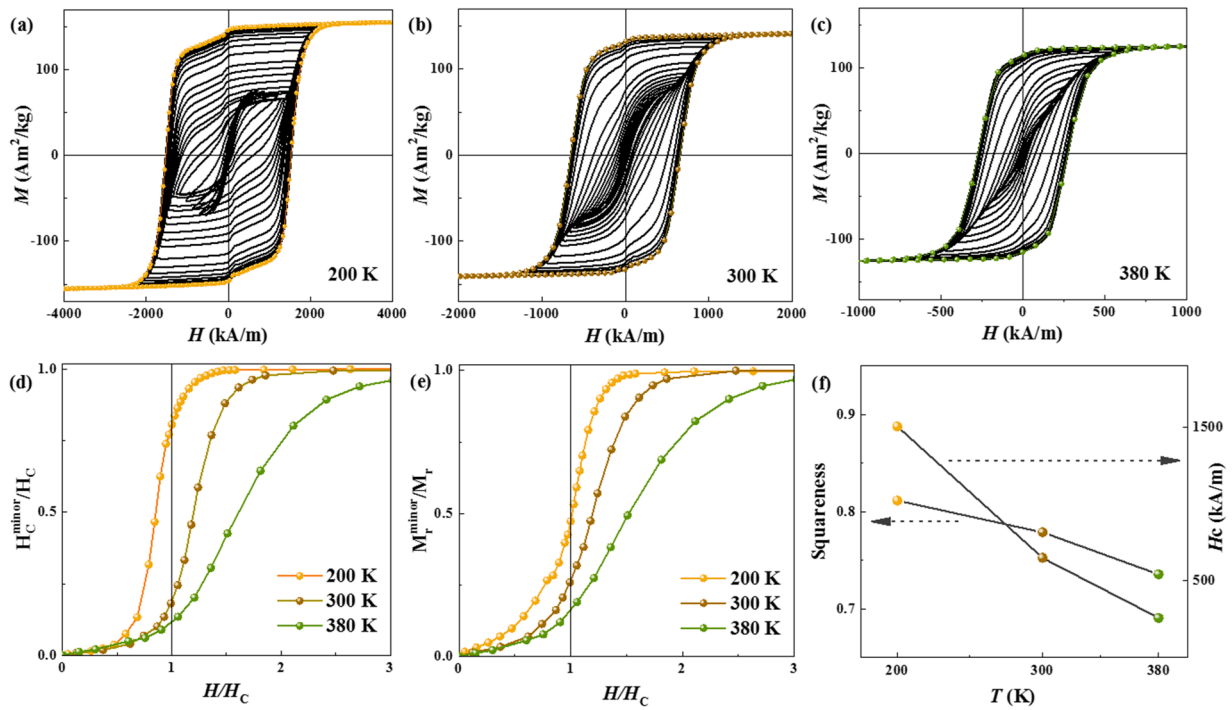
Fig. 4. Minor hysteresis loops of MM30 at temperatures of (a) 200 K, (b) 300 K and (c) 380 K. Trends of (d) normalized coercivity and (e) normalized remanence with the normalized external magnetic field. The horizontal and vertical coordinates are normalized with respect to the corresponding coercive field H_c. (f) Hysteresis loops of MM30 at different temperatures. Insets show the coercivity and squareness of the demagnetization curve as a function of temperature.
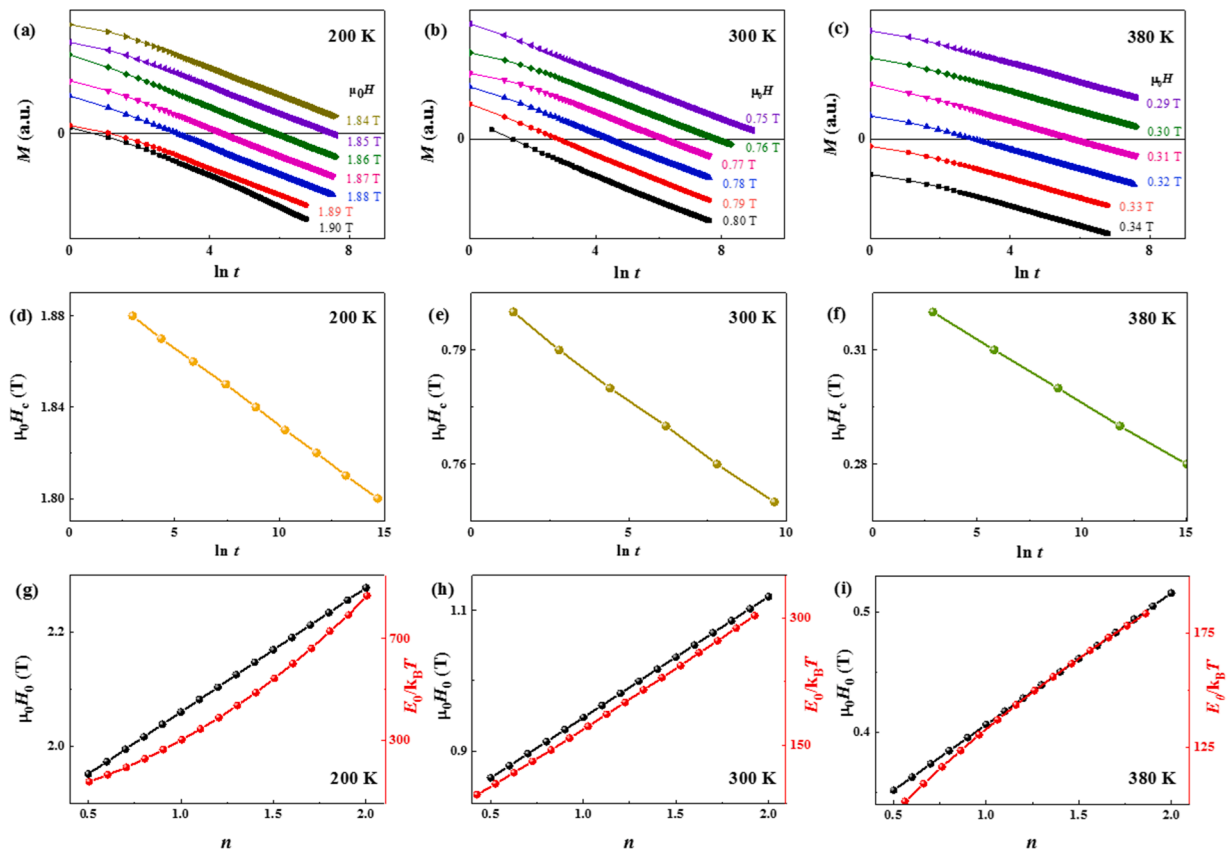
Fig. 5. (a)~(c) Time-dependent relaxation of magnetization under several external magnetic fields (near coercive field). (d)~(f) Relaxation of coercivity with time at different temperatures. (g)~(i) The coercivity and energy barrier without thermal disturbance as a function of exponent n.

the coercivity without thermal disturbance. The index n is related to the coercivity mechanism of the magnet, which is an effective way to identify the coercivity mechanism. The theoretical values of n are 2, 1.5 and 1 for uniform rotating, nucleating and domain wall pinning mechanisms.

For a magnet with an energy barrier of E_b, the perturbed magnetic field (H_f) caused by thermal perturbation for magnetization reversal is [34]:

$$H_f = -\frac{k_B T}{(\partial E_b / \partial H)}. \tag{7}$$

According to the thermal activation theory, thermal disturbance can be obtained by $H_f = S/\chi_{irr}$, where S is the magnetic viscosity coefficient and χ_{irr} is the irreversible susceptibility. The magnetization of the magnet will gradually decrease with time, as shown in Fig. 5(a)~(c). The time t required for the magnetization relaxation to zero is related to the external field as follows:

$$H(t) = H_0 \left\{ 1 - \left[\frac{k_B T}{E_0} \ln \frac{f_0 t}{0.693} \right]^{1/n} \right\}. \tag{8}$$

Where f_0 is the trial frequency of 10^{11} Hz. Fig. 5(d)~(f) shows that there is a good linear relationship between H_c and the logarithm of time $\ln t$. The variation of coercivity and energy barrier with n without thermal disturbance were obtained by numerical fitting. Compared with Eq. (6), the n values of 200 K, 300 K and 380 K can be determined to be 1.45, 1.18 and 1.0, respectively. It indicates that the magnets do have

different coercivity mechanisms at different temperatures. Consistent with the previous conclusions, the magnetization reversal is dominated by nucleation and pinning mechanism at 200 K and 380 K. However, the coercivity mechanism at 300 K is quite complex, and it is difficult to describe the magnetization reversal process by a single mechanism.

The coercivity mechanism of (MM,Nd)-Fe-B at 300 K was further studied to fully understand the process of magnetization and demagnetization of MMP magnets. Since the dependence of reversed magnetic field and angle θ (between the easy axis and the external field) can reflect different coercivity mechanisms, such as nucleation and pinning, the magnetization reversal processes at different θ were tested. As shown in Fig. 6(a) and (b), the H_R of two main phases and the coercivity of MM30 magnet increase with θ increases. It can be seen from Fig. 6(c) that the reversed field H_{Rpeak} corresponding to SFD peak moves toward the direction of high field when θ becomes larger. Especially when $\theta > 60°$, the peak value decreases rapidly and the distribution becomes more diffuse, that is, pinning effect is more obvious at large angles. However, FORC switching field distribution only changes slightly when θ is low, which has a great deviation from the angle relationship of the pinning mechanism. It also indicates that the external magnetic field will affect the magnetization reversal process of MM30 magnet at 300 K.

The demagnetization of MM30 magnets at 30° and 75° were also revealed by micromagnetic simulation. Multi-grain microstructure is constructed by centroidal Voronoi tessellation, which can better reflect the actual particle shape [35–37]. Fig. 6 is the magnetization reversal process of magnets under different external magnetic fields. The
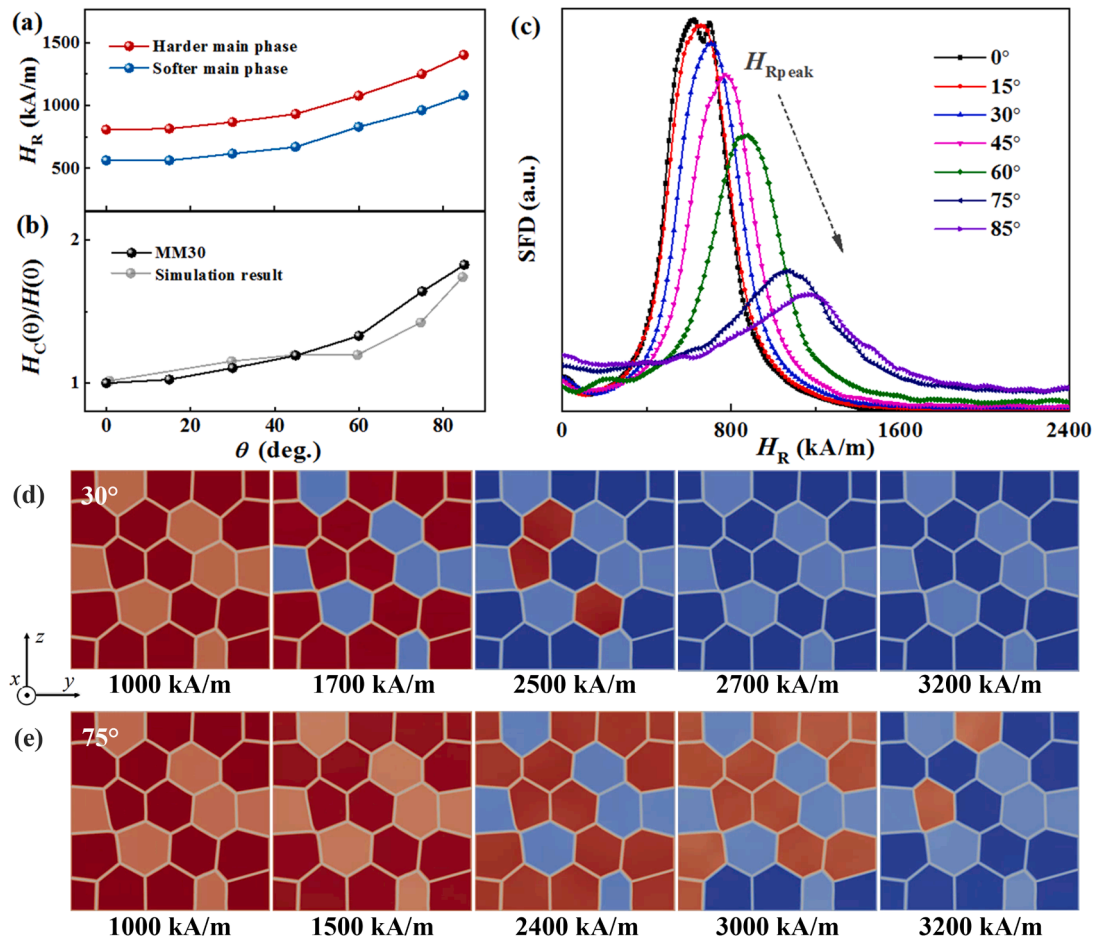
Fig. 6. (a) Reversed magnetic field of two main phases and (b) the coercivity of magnet as a function of angle θ between the easy axis and external field. (c) FORC switching field distribution (SFD) at different angles. Magnetization reversal process of MM30 magnet with magnetic field at (d) $\theta = 30°$ and (e) $\theta = 75°$. The magnetization in z-direction is represented by regions in red ($+z$) and blue ($-z$). (For interpretation of the references to colour in this figure legend, the reader is referred to the web version of this article.)

coercivity of the simulated magnet is generally higher than that of actual magnet, mainly because the grains are uniformly refined and there are no defects, which also indicates that the performance of MMP magnets can be further improved by forming better microstructure. The light colors (light red and light blue) represent the softer main phase, while the dark colors (dark red and dark blue) represent the harder main phase. As shown in Fig. 6(d), magnetization reversal occurs preferably inside the softer grains and then rapidly expands to the surrounding grains, resulting in magnetization reversal of the entire magnet. By comparing the domain configurations in Fig. 6 (e) and (d) under the same magnetic field, it can be seen that the reversed domain is difficult to be driven when the magnetic field is relatively small and swerve off the easy axis. Only the color of the magnet becomes lighter as the magnetic field increases, indicating that the magnetization changes very slowly. The weak exchange coupling inhibits the domain propagation between different phases, which makes the reversed domains nucleate mainly at the softer magnetic phase and boundaries. When the external magnetic field overcomes the pinning effect, the magnetic moments of the magnet are reversed and magnetized to saturation.

In addition, the intensity of reversed field will also affect the formation of effective exchange coupling between grains by affecting the domain directions of different grains. The second-order reversal curve (SORC) can be used to reflect the information of demagnetization under a specific reversed field H_{R1}. Fig. 7(a)~(c) are the SORCs of MM30 magnet at 300 K under -656 kA/m, -800 kA/m and -1600 kA/m. Two-dimensional SORC distribution is obtained according to the following equation [19]:

$$\rho(H_{R2}, H) = -\frac{1}{2M_s} \frac{\partial^2 M(H_{R1}, H_{R2}, H)}{\partial H_{R2} \partial H}. \tag{9}$$

Effective exchange coupling between two grains requires that the magnetic domains of MM-Fe-B grains are oriented in the same direction as all surrounding Nd-Fe-B grains. When the magnetic domains of MM-Fe-B and Nd-Fe-B grains are in opposite directions, the exchange coupling fails. As shown in Fig. 7, when $H_{R1} = $ -656 kA/m (around H_c), the domain directions of MM-Fe-B grains are not aligned with all the surrounding Nd-Fe-B grains, that is, the two grains cannot be coupled to each other. Since there is no effective exchange coupling and MM-Fe-B has a low reversed field, the peak of reversed field of most MM-Fe-B grain is near the zero magnetic field. There is only one peak in Fig. 7 (d) except the peak near zero field, which also indicates that the softer magnetic phase is completely decoupled from the harder one. The former reverses quickly at a very low field, while the latter has a reversed field of 880 kA/m. When $H_{R1} = $ -800 kA/m (slightly larger than H_c), the domain directions of some MM-Fe-B grains are aligned with all the surrounding Nd-Fe-B grains, that is, some of MM-Fe-B grains are coupled with Nd-Fe-B grains. Thus, the reversed field of the MM-Fe-B grains is increased to 400 kA/m. When $H_{R1} = $ -1600 kA/m (obviously larger than H_c), the domain directions of almost all MM-Fe-B grains are in the same direction as surrounding Nd-Fe-B grains. There is an effective exchange coupling between the two grains, and the reversed field of the MM-Fe-B grains is increased to 560 kA/m. The nucleation and propagation of reversed domains in most $MM_2Fe_{14}B$ grains are significantly suppressed by the exchange coupling with $Nd_2Fe_{14}B$ grains, which makes the magnetization reversal process of different grains more synchronous.

The magnetization reversal process of MM30 magnet at 300 K was clearly characterized in Fig. 8. Blue grains represent softer main phase with low anisotropy, while red grains represent harder main phase with high anisotropy. Assumed that softer magnetic phases are distributed around the harder magnetic phase and magnetized to saturation in a positive direction (Fig. 8(a)). The demagnetization process of magnet is represented longitudinally, and the recovery process of magnet is represented transversely. When the reversed field is very low, the two main phases are weakly coupled with each other. The magnetization reversal of the two phases is relatively independent, especially in the recovery process. As shown in Fig. 8(b) and (c), the softer magnetic phase reverses before the harder magnetic phase. When the reversed field increases, there is an effective exchange coupling between the two main phases. Grains with small anisotropy and those with large anisotropy are partially coupled and magnetized in the opposite direction. Coupled grains are also rotated uniformly during the recovery process. Fig. 8(d)
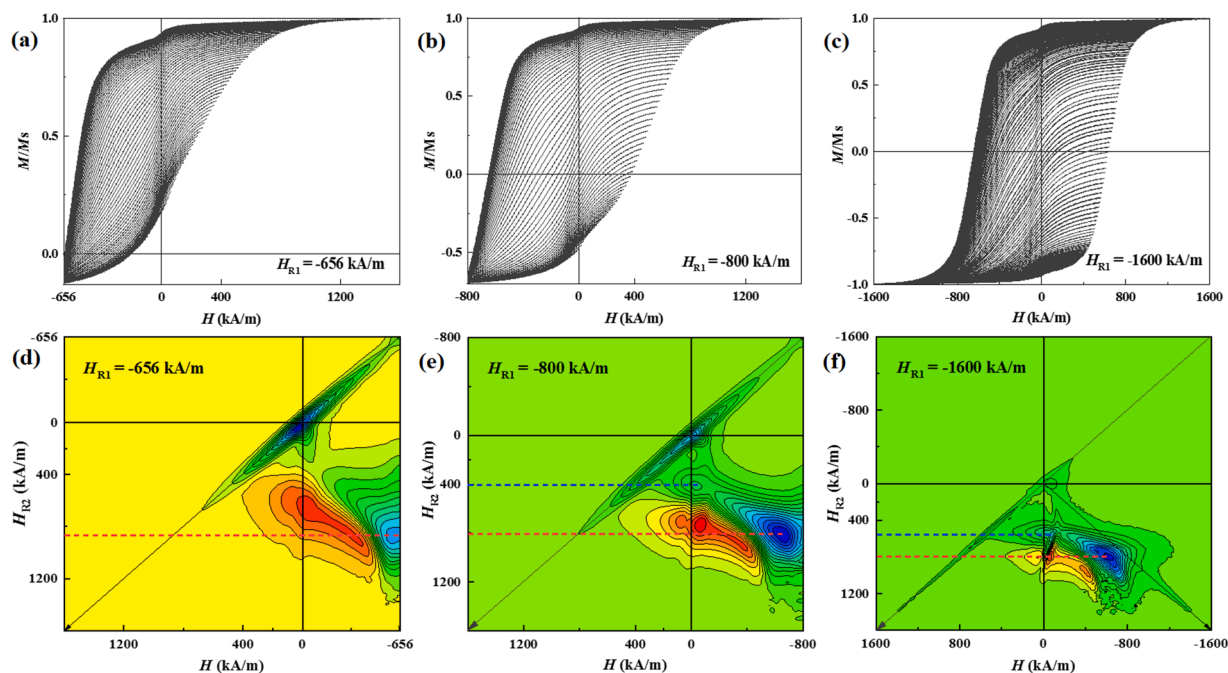
Fig. 7. The second-order reversal curve (SORC) of MM30 magnet at 300 K under different H_{R1}: (a) -656 kA/m, (b) -800 kA/m, and (c) -1600 kA/m. The corresponding SORC distribution (d), (e) and (f) are shown as two-dimensional contour maps with (H_{R2}, H) as the coordinates. The red and blue dashed lines correspond to the reversed magnetic field in which most $Nd_2Fe_{14}B$ and $MM_2Fe_{14}B$ grains are magnetized. (For interpretation of the references to colour in this figure legend, the reader is referred to the web version of this article.)
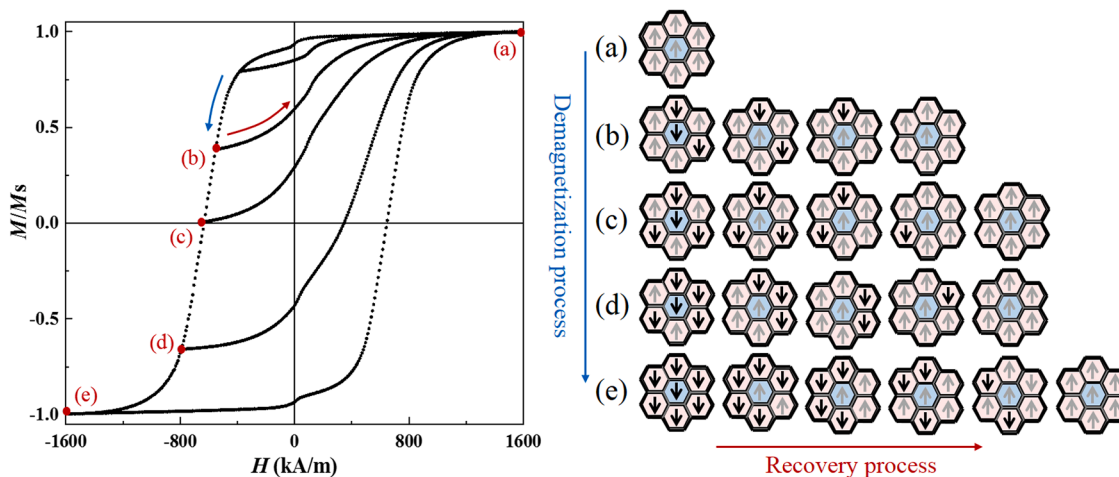
Fig. 8. (a)~(e) Schematic diagram of the demagnetization process and recovery process of MM30 sample at 300 K. The blue grains correspond to the softer magnetic phase, and the red grains correspond to the harder magnetic phase. The magnetization reversal of the magnet starts from the magnetization saturation state. (For interpretation of the references to colour in this figure legend, the reader is referred to the web version of this article.)

and (e) correspond to the situation in Fig. 7(e) and (f). The change in interaction results in the coexistence of two coercive mechanisms in the MMP magnet at 300 K. The effective exchange coupling between grains is affected by the domain directions of grains, which can be influenced by the applied magnetic fields. When the intensity of magnetic field or the angle with easy axis is large, the nucleation and diffusion of the reversed domain are hindered, and the pining mechanism dominates the magnetization reversal process.

4. Conclusions

In this paper, the magnetization reversal mechanism of MMP magnet is investigated by studying the interaction between the grains and the dynamic magnetization at different temperatures. It is found that the interaction is weakened with the increase of temperature, which makes the demagnetization process of softer and harder main phases becomes inconsistent. Compared with low temperature, the movements of magnetic moments are mainly affected by long-range magnetostatic interaction rather than exchange coupling at high temperature. According to the thermal activation theory, the *n* values related to the coercivity mechanism at 200 K, 300 K and 380 K are 1.45, 1.18 and 1.0, respectively. The main mechanism controlling the magnetization reversal process is the nucleation of reversed domains at low temperature and domain wall pinning at high temperature. However, the magnetization reversal of MMP magnet at 300 K is difficult to be described by a single coercivity mechanism. FORC with different angles and the corresponding 2D distributions confirm the coexistence of two coercivity mechanisms. Micromagnetism and SORC were also used to understand the coercivity mechanism of (MM,Nd)-Fe-B magnets sintered by dual alloy method, which is of great significance to improve the magnetic properties of high abundance rare earth magnets.

Declaration of Competing Interest

The authors declare that they have no known competing financial interests or personal relationships that could have appeared to influence the work reported in this paper.

Acknowledgments

References

[1] N. Jones, Materials science: the pull of stronger magnets, Nature 472 (2011) 22.

[2] C. Huber, H. Sepehri-Amin, M. Goertler, M. Groenefeld, I. Teliban, K. Hono, D. Suess, Coercivity enhancement of selective laser sintered NdFeB magnets by grain boundary infiltration, Acta Mater. 172 (2019) 66.

[3] Z.G. An, S.L. Li, L.C. Sun, J.Y. Zhang, Microstructure and magnetic properties of sintered Nd-Fe-B magnets with grain boundary diffusion Tb, Chin. J. Rare Met. 45 (2021) 34–40.

[4] X. Wang, Z.R. Zhao, F. Liu, Y.L. Liu, G.F. Wang, M.G. Zhu, X.F. Zhang, Phase composition and magnetic properties of Pr-Nd-MM-Fe-B nanocrystalline magnets prepared by spark plasma sintering, Rare Met. 1 (2020) 5.

[5] H. Chen, W. Liu, Z. Li, Y. Li, M. Yue, Optimizing microstructure and magnetic properties of mischmetal-based sintered magnets by grain refinement, Mater. Lett. 267 (2020), 127509.

[6] D. Liu, T.Y. Zhao, J.Y. Jin, T.Y. Ma, J.F. Xiong, B.G. Shen, F.X. Hu, J.R. Sun, Exchange interaction and demagnetization process of high abundance rare-earth magnets sintered using dual alloy method, Sci. China-Phys. Mech. Astron. 65 (4) (2022), 247511.

[7] T.Y. Ma, M. Yan, K.Y. Wu, B. Wu, X.L. Liu, X.J. Wang, Z.Y. Qian, C. Wu, W.X. Xia, Grain boundary restructuring of multi-main-phase Nd-Ce-Fe-B sintered magnets with Nd hydrides, Acta Mater. 142 (2018) 18.

[8] X.G. Cui, G.Y. Shu, J.X. Pan, J. Zhang, W.J. Liang, L.Z. Zhao, C.Y. Cui, T.Y. Ma, Z. H. Zhao, X.L. Peng, Enhanced magnetic properties and thermal stability of spark plasma sintered multi-main-phase Nd-Ce-Fe-B magnet via co-adding DyF3 and Cu, J. Alloys Compd. 902 (2022), 163786.

[9] H. Kronmüller, Theory of nucleation fields in inhomogeneous ferromagnets, Phys. Stat. Sol. (b) 144 (1987) 383–396.

[10] R. Ramesh, K. Srikrishna, Magnetization reversal in nucleation controlled magnets. I. theory, J. Appl. Phys. 64 (1988) 6406–6415.

[11] H. Chen, W.Q. Liu, Z.Z. Guo, T.Y. Yang, H.H. Wu, Y.Q.Y.Q. Li, H.G. Zhang, M. Yue, Coercivity enhancement of Nd-La-Ce-Fe-B sintered magnets: synergistic effects of grain boundary regulation and chemical heterogeneity, Acta Mater. 235 (2022), 118102.

[12] R. Ramesh, G. Thomas, B.M. Ma, Magnetization reversal in nucleation controlled magnets. II. Effect of grain size and size distribution on intrinsic coercivity of Fe–Nd–B magnets, J. Appl. Phys. 64 (1988) 6416–6423.

[13] J.J. Jin, T.Y. Ma, Y. Zhang, G. Bai, M. Yan, Chemically inhomogeneous RE-Fe-B permanent magnets with high figure of merit: solution to global rare earth criticality, Sci. Rep. 6 (2016) 32200.

[14] J.F. Xiong, R.X. Shang, Y.L. Liu, X. Zhao, W.L. Zuo, F.X. Hu, J.R. Sun, T.Y. Zhao, R. J. Chen, B.G. Shen, Magnetic properties of misch-metal partially substituted Nd–Fe–B magnets sintered by dual alloy method, Chin. Phys. B 27 (2018), 077504.

[15] R.K. Dumas, C.P. Li, I.V. Roshchin, I.K. Schuller, K. Liu, Magnetic fingerprints of sub-100 nm Fe dots, Phys. Rev. B 75 (2007) 34405.

[16] J.E. Davies, O. Hellwig, E.E. Fullerton, G. Denbeaux, J.B. Kortright, K. Liu, Magnetization reversal of Co/Pt multilayers: microscopic origin of high-fieldmagnetic irreversibility, Phys. Rev. B 70 (2004), 224434.

[17] J.E. Davies, O. Hellwig, E.E. Fullerton, J.S. Jiang, S.D. Bader, G.T. Zimanyi, K. Liu, Anisotropy dependence of irreversible switching in Fe/SmCo and FeNi/FePt exchange spring magnet films, Appl. Phys. Lett. 86 (2005), 262503.

[18] I.D. Mayergoyz, G. Friedmann, Generalized Preisach model of hysteresis, IEEE Trans. Magn. 24 (1988) 212.

[19] I. Bodale, L. Stoleriu, A. Stancu, Reversible and irreversible components evaluation in hysteretic processes using first and second-order magnetization curves, IEEE Trans. Magn. 47 (2011) 192–197.

[20] D. Givord, Q. Lu, F.P. Missell, M.F. Rossignol, D.W. Taylor, V. Villas Boas, A direct study of the dipolar field in several RFeB systems, J. Magn. Magn. Mater. 104-107 (1992) 1129–1131.

[21] D.W. Taylor, V. Villas-Boas, Q. Lu, M.F. Rossignol, F.P. Missell, D. Givord, S. Hirosawa, Coercivity analysis in $R_{17}Fes_{83-x}B_x$ magnets, J. Magn. Magn. Mater. 130 (1994) 225–236.

[22] A. Bolyachkin, H. Sepehri-Amin, I. Suzuki, H. Tajiri, Y.K. Takahashi, K. Srinivasan, H. Ho, H. Yuan, T. Seki, A. Ajan, K. Hono, Transmission electron microscopy image based micromagnetic simulations for optimizing nanostructure of FePt-X heat-assisted magnetic recording media, Acta Mater. 227 (2022), 117744.

[23] D. Liu, S.D. Jiang, L.C. Wang, R.S. Liu, M. Zhang, T.Y. Zhao, F.X. Hu, J.R. Sun, B.G. Shen, Spontaneous magnetization and magnetic domain texture of strontium hexaferrite in equilibrium state, Rare Met. 41 (2022) 3019–3026.

[24] P.E. Kelly, K. O'Grady, P.I. Mayo, R.W. Chantrell, Switchingmechanismsin cobalt–phosphorus thin films, IEEE Trans. Magn. 25 (1989) 3881–3883.

[25] R. Quey, P.R. Dawson, F. Barbe, Large-scale 3D random polycrystals for the finite element method: generation, meshing and remeshing, Comput. Methods Appl. Mech. Eng. 200 (2011) 1729–1745.

[26] W. Scholz, J. Fidler, T. Schrefl, D. Suess, R. Dittrich, H. Forster, V. Tsiantos, Scalable parallel micromagnetic solvers for magnetic nanostructures, Comput. Mater. Sci. 13 (2003) 366–383.

[27] C. Geuzaine, J.F. Remacle, Gmsh: a three-dimensional finite element mesh generator with built-in pre-and post-processing facilities, Int. Int. J. Numer. Methods Eng. 79 (1997) 1309–1331.

[28] T. Schrefl, R. Fischer, J. Fidler, H. Kronmüller, Two- and three-dimensional calculation of remanence enhancement of rare-earth based composite magnets, J. Appl. Phys. 76 (1994) 7053–7058.

[29] J.F. Herbst, $R_2Fe_{14}B$ materials: intrinsic properties and technological aspects, Rev. Mod. Phys. 63 (1991) 819–898.

[30] C.R. Pike, A.P. Roberts, K.L. Verosub, Characterizing interactions in fine magnetic particle systems using first order reversal curves, J. Appl. Phys. 85 (1999) 6660.

[31] H.G. Katzgraber, F. Pazmandi, C.R. Pike, K. Liu, R.T. Scalettar, K.L. Verosub, G.T. Zimanyi, Reversal-field memory in the hysteresis of spin glasse, Phys. Rev. Lett. 89 (2002), 257202.

[32] S. Okamoto, K. Miyazawa, T. Yomogita, N. Kikuchi, A. Kato, Temperature dependent magnetization reversal process of a Ga-doped Nd-Fe-B sintered magnet based on first-order reversal curve analysis, Acta Mater. 178 (2019) 90.

[33] R. Goto, S. Okamoto, N. Kikuchi, O. Kitakami, Energy barrier analysis of Nd-Fe-B thin films, J. Appl. Phys. 117 (2015) 17B514.

[34] Y. Estrin, P.G. McCormick, R. Street, A phenomenological model of magnetisation kinetics, J. Phys. 1 (1989) 4845–4851.

[35] D. Liu, T.Y. Ma, L.C. Wang, Y.L. Liu, T.Y. Zhao, F.X. Hu, J.R. Sun, B.G. Shen, J. Phys. D: Appl. Phys. 52 (13) (2019), 135002.

[36] Q. Du, V. Faber, M. Gunzburger, Centroidal Voronoi tesselations: applications and algorithms, Siam. Rev. 41 (1999) 637.

[37] J. Kim, S. Torquato, New Tessellation-based procedure to design perfectly hyperuniform disordered dispersions for materials discovery, Acta Mater. 168 (2019) 143–151.